ACS APPLIED MATERIALS & INTERFACES

www.acsami.org

Research Article

3D Printing Magnetic Actuators for Biomimetic Applications

Xufeng Cao, Shouhu Xuan,* Shuaishuai Sun, Zhenbang Xu, Jun Li, and Xinglong Gong*

Cite This: *ACS Appl. Mater. Interfaces* 2021, 13, 30127−30136

Read Online

ACCESS | Metrics & More | Article Recommendations | Supporting Information

ABSTRACT: Biomimetic actuators with stimuli-responsiveness, adaptivity, and designability have attracted extensive attention. Recently, soft intelligent actuators based on stimuli-responsive materials have been gradually developed, but it is still challenging to achieve various shape manipulations of actuators through a simple 3D printing technology. In this paper, a 3D printing strategy based on magneto-active materials is developed to manufacture various biomimetic magnetic actuators, in which the new printable magnetic filament is composed of a thermoplastic rubber material and magnetic particles. The continuous shape transformation of magnetic actuators is further demonstrated to imitate the motion characteristic of creatures, including the predation behavior of octopus tentacles, the flying behavior of the butterfly, and the flower blooming behavior of the plant. Furthermore, the magnetic field-induced deformation of the biomimetic structure can be simulated by the finite element method, which can further guide the structural design of the actuators. This work proves that the biomimetic actuator based on soft magneto-active materials has the advantages of programmable integrated structure, rapid prototyping, remote noncontact actuation, and rapid magnetic response. As a result, this 3D printing method possesses broad application prospects in soft robotics and other fields.

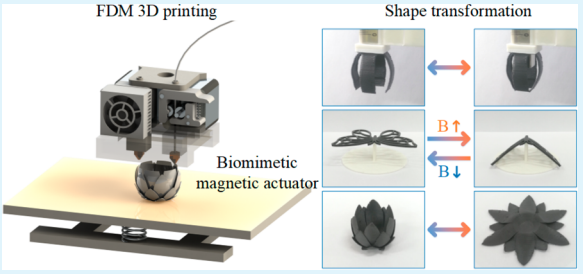

KEYWORDS: *smart materials, magnetic actuation, 3D print, actuator, biomimetic structure*

1. INTRODUCTION

Inspired by natural biology, soft actuators with stimuli-responsiveness, adaptability, and designability have attracted extensive attention. Compared with traditional rigid actuators, soft actuators have the advantages of simple structure, silent operation, good flexibility, and biocompatibility. In this field, the smart actuators based on stimulus-response materials are highly desirable, which can generate various mechanical deformation quickly and gently under different external stimuli. Stimulus-response materials based on various actuation principles have been widely applied in soft actuators, including light,[1,2] electric,[3,4] heat,[5,6] magnetic,[7−9] pneumatic,[10,11] and chemical[12,13] stimulus. Among these actuation principles, magnetic actuation is one of the most attractive actuation methods because the magnetic field can easily and harmlessly penetrate most biological materials and provide a fast and effective actuation method,[14,15] which has also been proven to be safe for humans in magnetic resonance imaging and magnetic hyperthermia. Magneto-active materials composed of magnetic particles and flexible polymer matrix[16] are widely used in various fields due to the advantages of simple control, rapid response, and remote contactless actuation. Among them, soft-magnetic materials utilize carbonyl iron particles with low-remanence and low-coercivity to achieve a high response of the structural deformation to the magnetic field.[17] Upon applying the magnetic field, a large macroscopic deformation can be obtained due to the magnetic interaction force between the magnetic particles and the magnetic field. After removing the external magnetic field, the reconfigurable magneto-active materials can recover to the original state due to their inherent elasticity and reversible properties. Recently, many soft smart actuators based on magneto-active materials have been developed,[18−20] and they exhibited high performance on shape transformation of magnetic kirigami patterns and remote actuation of magnetically actuated lifters, accordions, valves, pumps, and mixers.

Because of the complex structure, the traditional molding method is limited in manufacturing magnetic actuators. 3D printing technology is a kind of additive manufacturing technology, which has been successfully applied in various fields.[21−24] For the new generation magnetic actuators, the development of different printing strategies based on various matrix materials is of paramount importance due to the wide diversity of 3D printing structures. Recently, with the development of printing materials, many magnetic actuators with novel design concepts based on 3D printing technology have been developed, including digital light processing (DLP),[25−30] direct ink writing (DIW),[31−36] and fused deposition modeling (FDM).[37−40] 3D printing magnetic actuators can be divided

Received: May 5, 2021
Accepted: June 9, 2021
Published: June 17, 2021

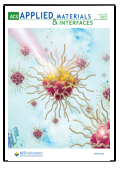

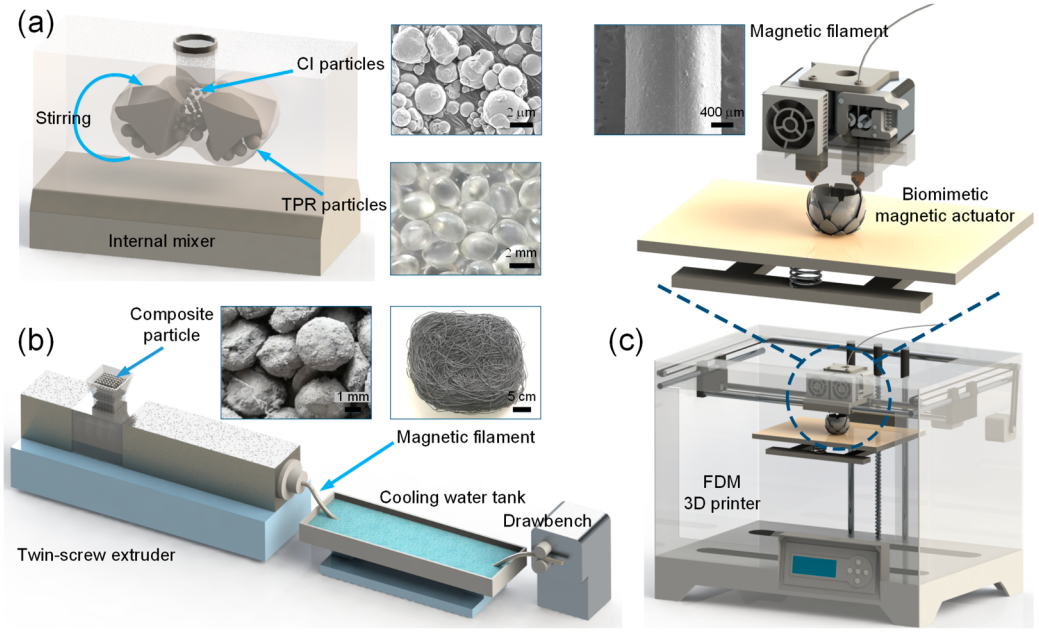

Figure 1. Schematic illustration of (a,b) the fabrication processes of magnetic filaments and (c) the printing processes of the biomimetic magnetic actuator.

into structures based on homogeneously dispersed soft magnetic particles[32,33] or structures based on anisotropic magnetization profiles.[28,31,35,36] The latter is achieved by patterning magnetic particles or magnetizing hard magnetic particles in the matrix. These actuators will be subjected to force or torque under the magnetic actuating field thus resulting in shape transformation.[41,42] Furthermore, the diversity of the 3D printing method can promote the development of magnetic actuators. Among them, in comparison to the DLP, FDM has the advantages of a simple working principle, no particle sedimentation, wide adaptability of material, and low cost. Moreover, during the DIW printing process, due to the low initial modulus of the ink, the actuators will collapse and deform under the action of gravity when printing the three-dimensional structure. To our knowledge, most of the previously printed magnetic actuators were 2D and 2.5D structures, even a few of them were soft magnetic actuators with a complex structure. As a result, it is still a challenge to realize a simple 3D printing technology for soft actuators with magnetic shape manipulations. However, in the FDM method, since the filament has a relatively large modulus compared with the ink and the material is cooled rapidly during the printing process, three-dimensional structures can be directly printed. As a result, FDM printing based on flexible magneto-active materials is one of the effective and feasible solutions, in which thermoplastic rubber (TPR) with both rubber and thermoplastic properties is an ideal matrix material.

Herein, a 3D printing strategy is developed for biomimetic magnetic actuators, in which a new printable magnetic filament composed of thermoplastic rubber material and magnetic particles is employed as the magneto-active materials. Inspired by natural creatures, various biomimetic magnetic actuators were printed to imitate their motion characteristics, including the predation behavior of octopus tentacles, the flying behavior of the butterfly, and the flower blooming behavior of the plant. It is found that the magnetic field-dependent deformation of the magneto-active materials dominated the final actuation. The finite element method (FEM) is employed to simulate the magnetic field-induced deformation of biomimetic actuators and the simulation matches well with the experiment results. This research is helpful in promoting the development of biomimetic actuators with programmable integrated structure and good controllability, which further provides a wide application potential of magneto-active materials in soft intelligent robots, biomedicine, and bionics.

2. MATERIAL AND METHODS

2.1. Materials. The thermoplastic rubber (TPR) particles with a shore hardness of 70A used as the flexible matrix were supplied by the Hanwha TOTAL Petrochemical Co., Ltd. As the magnetic filler, the carbonyl iron particles (CIPs, 7 μm average diameter) were purchased from BASF in Germany. TPR particles and CIPs were dried at 50 °C for 10 h before the fabrication process.

2.2. Fabrication and Printing Processes. The fabrication and printing processes of the biomimetic magnetic actuator were shown in Figure 1. As illustrated in Figure 1a, the TPR particles were first heated to 70 °C in the internal mixer to soften the surface, and then the CIPs with the same mass were slowly added for premixing. The composites were obtained after thoroughly stirring. Then, a twin-screw extruder was used to fabricate the magnetic filaments with CIPs content of 50 wt % (Figure 1b). The above composites were poured into the feed hopper and then flowed downward into the extruder barrel. After thoroughly mixing in the screw extruder at 190 °C, the molten mixture was cooled by water after coming out of the die. By using the appropriate feeding speed, screw speed, and drawing speed of the drawbench, the appropriate magnetic filaments with the required diameter of 1.7−1.8 mm which could be fed into the 3D printer smoothly were obtained. Finally, the biomimetic magnetic actuators were printed by utilizing an FDM 3D printer (Figure 1c).

2.3. Characterization. The microscopic morphology of filaments and printed films were observed by using scanning electron microscopy (SEM, GeminiSEM 500, ZEISS). The magnetic properties of filaments were characterized using a Hysteresis Measurement of Soft and Hard Magnetic materials (HyMDC Metis, Leuven, Belgium). The tensile performance of filaments and printed films with rectangle shape were obtained by a dynamic mechanical analyzer (DMA, ElectroForce 3200, TA Instruments, USA). The loading rate was set at 0.1 mm/s. Besides, the magnetic field, generated by a NdFeB permanent magnet, commercial electromagnet, and DC power, was measured by a Tesla meter (HT20, Shanghai Hengtong Magnetic Technology Co., Ltd.,

https://doi.org/10.1021/acsami.1c08252
ACS Appl. Mater. Interfaces 2021, 13, 30127−30136

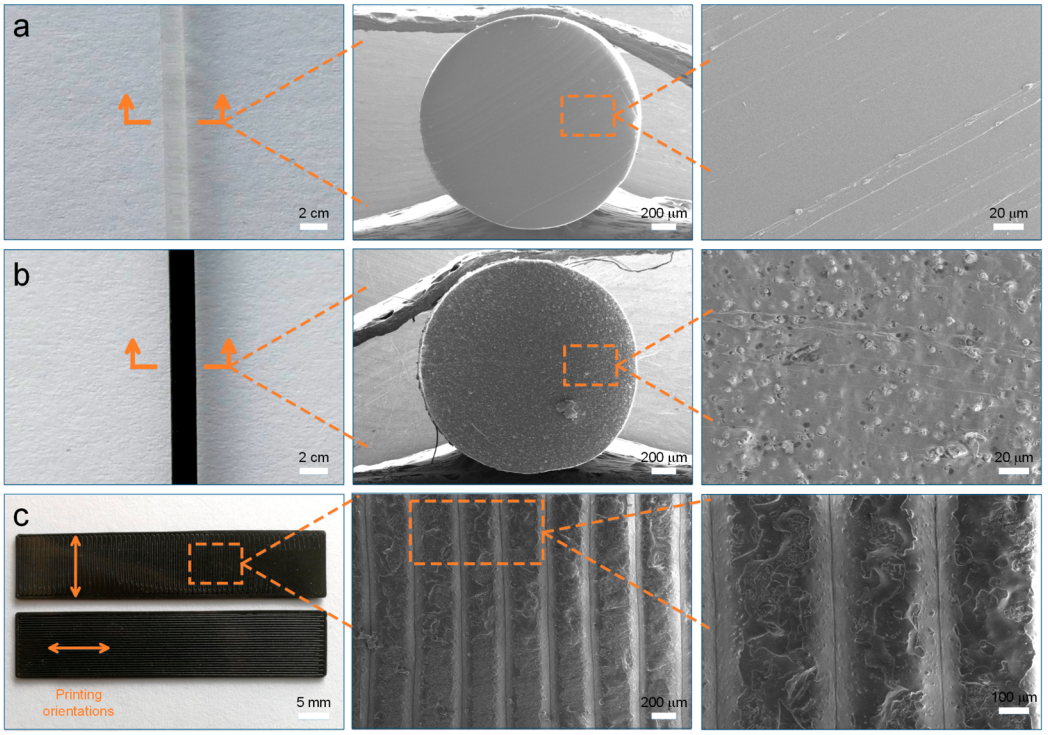

Figure 2. Digital images, SEM micrographs, and its magnified images for (a) the cross-section of the pure TPR filament, (b) the cross-section of the magnetic filament, and (c) the surface of the printed films.

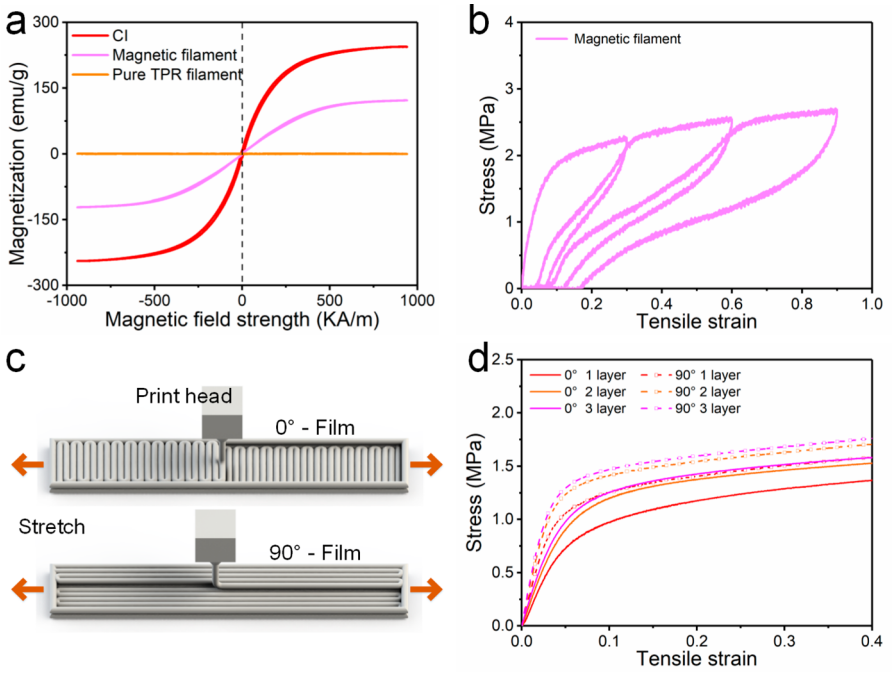

Figure 3. (a) Magnetization curves of CIPs, magnetic filament, and pure TPR filament. (b) Tensile stress−strain curves for the magnetic filament. (c) Schematic illustration of the printing orientations. (d) Tensile stress−strain curves for the printed TPR/CIPs films with different printing orientations and the number of layers.

China). FDM 3D printing was completed by using a commercial 3D printer (Creator pro, Flashforge Co., China).

2.4. Numerical Methods. The finite element method (FEM) was adopted to calculate the deformation characteristics of the biomimetic magnetic actuator. The simulation was carried out by COMSOL Multiphysics 5.4. The geometric models were first designed by SolidWorks 2016 and directly imported into COMSOL. The geometry included the solid domain and air domain. Each domain was defined by the corresponding material properties. The magnetic force on the magnetic actuator was imported from the force calculation interface. The fixed support was applied to the corresponding position of the magnetic actuator. In the case of small strain and large rotation, the nonlinear solver settings option was open. After proper meshing and solving, the deformation characteristics of the biomimetic magnetic actuator could be obtained.

https://doi.org/10.1021/acsami.1c08252
ACS Appl. Mater. Interfaces 2021, 13, 30127−30136

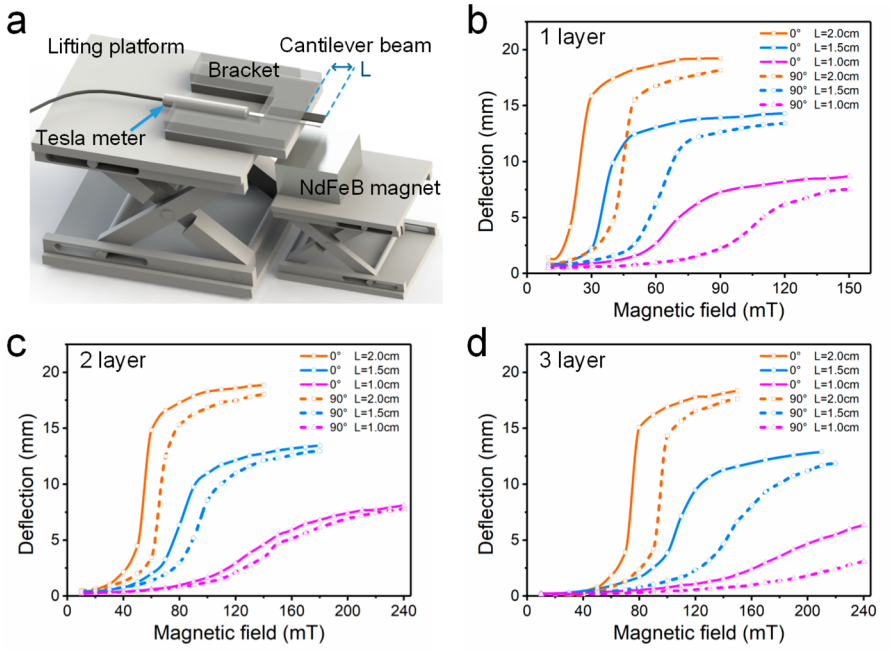

Figure 4. (a) Schematic illustration of the cantilever beam test system. (b–d) The deflection versus the magnetic field curves of the cantilever beam with different printing orientations and the number of layers.

3. RESULTS AND DISCUSSION

3.1. Characterization for the Filament and Printed Film. TPR/CIPs composite with good thermoplasticity and high flexibility was an ideal raw material for fabricating magnetic filaments with a diameter of 1.7–1.8 mm. High printing accuracy could be obtained by adjusting and optimizing the printing parameters. The nozzle diameter was 0.8 mm. During the printing process, printing speed, layer height, and infill density were set to be 10 mm/s, 0.2 mm, and 100%, respectively. Besides, the nozzle temperature and build-plate temperature were set at 210 and 70 °C. The deposition directions of the infill pattern for layers were 0° or 90°. Figure 2 showed the digital images and the SEM micrographs of the pristine filament and the final printed film. As illustrated in Figure 2a, the pure TPR filament was neat and homogeneous. After doping the black CIPs, the magnetic filament became a black color. Figure 2b showed the SEM images of the cross-section of the magnetic filament, which indicated that the CIPs were uniformly distributed within the TPR and the surface bonding capabilities between the CIPs and TPR matrix were very good. Here, the filament could be used to fabricate various structures *via* the 3D printing technique. As shown in Figure 2c, the magnetic films were easily obtained by the above method and they showed different fiber structures by varying the printing orientations. Besides, the SEM micrographs for the surface of the printed film were also studied. Obviously, it had few inconsistencies within the intralayer regions, indicating a good printability of this method. Moreover, the adhesion between the printed fibers was relatively strong, which endowed the printed product with a good mechanical property.

The hysteresis loop showed the saturation magnetization of CIPs, magnetic filament and pure TPR filament was about 245, 123, and 0 emu/g, respectively (Figure 3a). The residual magnetization and coercivities were almost zero, which allowed the magnetic filament with easy changes in the magnetic properties. The cyclic tensile stress–strain curves of the magnetic filament were illustrated in Figure 3b. In the cyclic loading stage, the displacement was applied to achieve the specified strain (30%, 60%, and 90%), and then the displacement was returned to the original position before the beginning of the next loading cycle. As expected, the stress–strain curve depended on the maximum loading encountered previously. Obviously, the as-prepared magnetic filament exhibited a typical Mullins effect. During the cyclic loading stage, if the load was less than the previous maximum load, the stress would be much lower than the stress of the first load process, and it exhibited nonlinear elastic behavior. When the loading increased beyond its previous maximum load, the stress–strain curve would return to the linear elastic curve.

To study the effect of the printing orientations (0° and 90°) and the number of layers (1, 2, and 3 layers) on the mechanical properties, films with different thicknesses (0.34, 0.54, and 0.74 mm) were printed in two printing orientations: 0° film and 90° film. The length and width of the films were 50 and 10 mm, respectively. For the 0° film, the printing orientation was the same as the width direction (Figure 3c). While for the 90° film, the printing orientation was the same as the length direction (Figure 3c). All samples were tested with the tensile direction along the length direction. Figure 3d showed the comparison of the tensile strain–stress curves for the printed films with different printing orientations and the number of layers. The initial 3% strain region was used to calculate the modulus, where the stress–strain relationship was linear. This result showed that for films with the same number of layers, the tensile modulus of the 0° films (17.3, 21.3, and 23.7 MPa for 1, 2, and 3 layers, respectively) was always less than the 90° films (27.7, 32.8, and 34.1 MPa for 1, 2, and 3 layers, respectively). This was because there were more printed fibers adhesion of the 0° film in an individual layer. The larger contact area among the printed fibers increased the probability of voids and imperfect bonding, which inevitably led to a smaller tensile modulus. Besides, keeping the same printing orientation, the tensile modulus increased with the number of layers. The reason for this phenomenon may be that when printing the next layer, some materials in the previous

https://doi.org/10.1021/acsami.1c08252
ACS Appl. Mater. Interfaces 2021, 13, 30127–30136

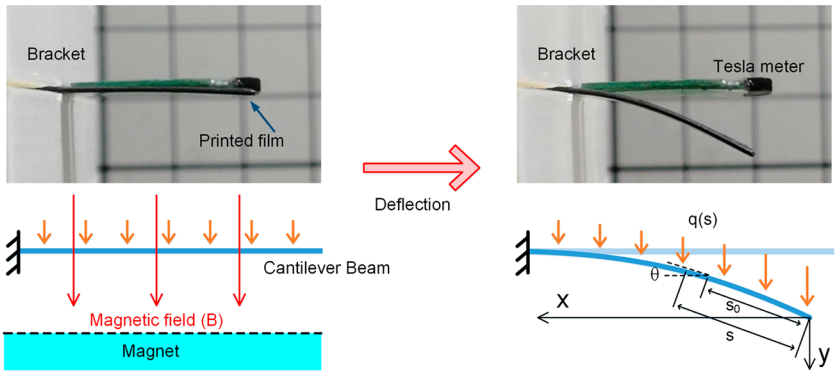

Figure 5. Digital images and schematic diagram of the magnetic field-induced deformation process for the printed film. (x, y) and (s, θ) denoted rectangular and curvilinear coordinates, respectively.

layer could be melted to reduce the voids and defects. Finally, compared with the magnetic filament (36 MPa, Figure 3b), the strength of all the printed films was slightly decreased due to the voids and imperfect bonding during the printing process.

To investigate the bend deformation behavior of printed films with different printing orientations and the number of printing layers, a cantilever beam bending test was carried out. Figure 4a showed the schematic diagram of the test system. The structure and size of the test samples were the same as the previous tensile specimens. The magnetic field strength around the cantilever beam was controlled by moving the height position of the NdFeB magnet (N52, 50 × 50 × 30 mm) and was monitored in real time by a Tesla meter probe at the same height as the beam. At the same time, a camera was used to record the bending deformation of the beam, and the deformation was measured by the analysis software. For convenience, the length of the cantilever beam was defined as L, and the deflection was defined as the vertical displacement of the end of the beam.

Figure 4b–d showed the deflection deformation versus the applied magnetic field curves for the cantilever beam. The curves could be divided into three stages: in the first stage, the deflection slowly increased with the magnetic field strength. When the magnetic field was applied to the cantilever beam, the magnetic force was generated along the thickness of the cantilever beam, which increased with the magnetic field. In the second stage, with further increasing of the magnetic field, the deflection of the cantilever beam increased sharply. This was because the magnetic field around the beam showed a nonlinear increase as the magnet approached. Therefore, the magnetic interaction force was increased accordingly, and the nonlinear magnetic force distribution caused a larger deformation. In the last stage, the maximum deflection deformation close to the film length would be obtained in the balance stage, and the bending angle of the cantilever beam could reach close to 90° at this time. Furthermore, consistent with the tensile experiment (Figure 3d), for the cantilever beams with the same test length and number of layers, the 0° film was always easy to generate large deflection deformation than the 90° film. Figure 4b–d also showed that with the same number of layers, the longer beam could generate larger deformation under the same magnetic field. Due to low bending stiffness, the relatively thin beam was also more sensitive to deformation than other thick beams. In a word, all the printing orientation, length, and thickness affected the deflection of the cantilever beam under the magnetic field. Therefore, through different parameter combinations, the deformation magnitude of the printed magnetic actuator under different magnetic fields could be designed.

To better understand the deformation mechanism, the printed film was adopted as a simplified theoretical model to demonstrate its magnetic response behavior under the magnetic field (Figure 5). For the isotropic TPR/CIPs composite material, which could be magnetized under the external magnetic field, the relationship between magnetization M and magnetic field H was $M = (u_r - 1)H$, where u_r was the relative permeability. Because the magnetic property of the composite materials was determined only by CIPs content, the relative permeability could be calculated by $u_r = 1 + \frac{3ø(4+ø)}{4(1-ø)}$[43] and the ø was the volume fraction of magnetic particles. The magnetic flux density B could be obtained by $B = \mu_0(H + M)$, where μ_0 was the permeability of vacuum. Then, the magnetization of the composite materials could be expressed as $M = (u_r - 1)H = \frac{(u_r - 1)}{u_0 u_r}B$. Furthermore, the magnetic force applied on the beam could be determined by $f_m = M \cdot \nabla B$.[42] The length, width, and thickness of the cantilever beam were l, m, and n, respectively. Thus, combining the equations above, the magnetic field load q along the length direction of the beam could be calculated as

$$q = f_m mn = \frac{mn(u_r - 1)}{u_0 u_r} B\partial B \tag{1}$$

After deformation, the shape of the beam was schematically shown in Figure 5, where the direction of the load was consistent with the initial state. Herein, (x, y) and (s, θ) were used to denote the rectangular coordinates and the curvilinear coordinates, respectively. Due to the same origin at the free end, the geometric relationship could be expressed as $dx = \cos\theta\, ds$ and $dy = \sin\theta\, ds$. Usually, the length of the beam was assumed to remain constant. Therefore, the deflection differential equation of the beam could be written as

$$\mathrm{EI}\frac{d\theta}{ds} = -\int_0^s q(s_0)\left[\int_{s_0}^s \cos\theta(s_1)ds_1\right]ds_0 \tag{2}$$

where EI was the bending stiffness of the beam. According to the calculus theory, we take the derivative of the equation again:

$$\mathrm{EI}\theta'' + \cos\theta\int_0^s q(s_1)ds_1 = 0 \tag{3}$$

where the boundary conditions were $\theta(l) = 0$ and $\theta'(0) = 0$. Eq 3 was typical boundary value problems of nonlinear ordinary differential equations, which was usually solved by the numerical calculation of the shooting method. After obtaining the equation

https://doi.org/10.1021/acsami.1c08252
ACS Appl. Mater. Interfaces 2021, 13, 30127−30136

of θ with respect to s, the coordinates of any point on the beam could be obtained by $x(s) = \int_0^s \cos\theta \, ds$, $y(s) = \int_0^s \sin\theta \, ds$. Here, the load q was first obtained based on the initial conditions. However, the load in the nonuniform magnetic field would change with the deformation of the beam, which was called magneto-elastic coupling. To solve the coupled problem, an iterative algorithm was needed to solve eqs 1 and 3 repeatedly. The solution process was mathematically complicated and difficult, but the FEM was perfectly fitted to the solution of this kind of problem. Thus, we would utilize finite element simulation to obtain the magnetic field-induced deformation of the complex structures under various magnetic fields.

As a result, the physical principle of determining the magnetic response behavior was very simple: the structure was driven and controlled by the magnetic force under the external magnetic field, and the final shape was balanced by the magnetic force and the elastic interaction force. After removing the magnetic field, the structure would return to the original shape, which was driven by the deformation-induced elastic energy.

3.2. Magnetic Actuation Deformation of the 3D Printed Biomimetic Magnetic Actuator. Both two-dimensional and three-dimensional complex structures have been successfully constructed, which demonstrated the versatility of FDM 3D printing technology. Figure 6 showed the digital images of the various 3D printed structures, including polygon, polyhedron, three-dimensional geometric structure, inchworm-like structure, gearwheel-like structure, drum-like structure, and honeycomb structure. The surface of the printed structure was delicate, smooth, and continuous and showed that the TPR/CIPs magnetic filament was suitable for the 3D structure printing by the FDM technology. On the basis of the above result, it could be concluded that the good printability of magnetic filaments ensured it to be applied for printing the magnetic actuators with complex structures.

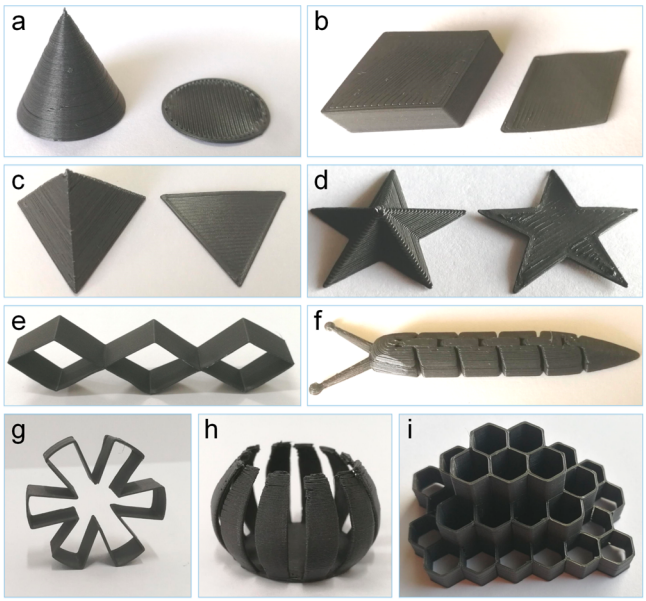

Figure 6. Digital images of the various 3D printed structures, including polyhedron and polygon for (a) cone and circle, (b) prism and rhombus, (c) tetrahedron and triangle, (d) 3D pentagram and pentagram, (e) continuous prismatic structure, (f) inchworm-like structure, (g) gearwheel-like structure, (h) drum-like structure, and (i) honeycomb structure.

Inspired by the predation behavior of octopus tentacles, a tentacle-like biomimetic magnetic actuator was designed and printed to demonstrate the movement characteristics of the real tentacles. Figure 7a showed the structural design of the four-arm tentacle-like actuator and the way of the magnetic field loading. First, the top of the actuator was fixed on the bracket, and then a NdFeB magnet (N35, $10 \times 10 \times 50$ mm) was placed through the actuator to provide the external magnetic field. By vertical moving the NdFeB magnet up and down, a variable magnetic field could be obtained to provide the magnetic actuation. The digital images and video of the movement process of the magnetic actuator were recorded by the camera. Here, the deflection was defined as the horizontal displacement of the end of the arm.

Figure 8 briefly showed the grasping and releasing movement process of the tentacle-like biomimetic magnetic actuator. During the downward movement of the magnet, the tentacle would bend to the side of the magnet under the action of the magnetic force and finally reached the closed state with increasing of the magnetic field. By moving the magnet up, the tentacle recovered to its original shape under the action of the inherent elasticity of the material. This result showed the printed biomimetic actuator based on a magnetic filament had the flexibility of the TPR matrix, which could deform by the remotely controllable magnetic force. Note that the strength of the structure could be increased by increasing the number of printed layers, and a larger magnetic field was required to drive the thicker one. Video S1 showed the movement process of the tentacle-like actuator and it was found that the grasping and releasing movement could be controlled continuously, quickly, and reversibly by magnetic actuation. Furthermore, the movement process for the actuator was analyzed through FEM. The simulation results had a similar variation tendency to the experimental values (Figure 7d), indicating that the simulation model could qualitatively predict the deformation of the actuator. In another word, the rapid and reversible actuation of the actuator based on magneto-active material could realize reconfigurable grasping actions. The successful application of FDM 3D printing technology in the manufacture of biomimetic magnetic actuators provided a promising strategy for integrated printing molding of actuators.

Inspired by the flying behavior of the butterfly, a corresponding butterfly-like biomimetic magnetic actuator was designed and printed to imitate the movement characteristics of the real butterfly. As illustrated in Figure 7b, the central body of the butterfly actuator was fixed on the bracket, and an electromagnet was placed directly under the bracket to provide a periodic magnetic field. By uniformly increasing and decreasing the current, the corresponding magnetic interaction force could be obtained as a magnetic excitation. The magnetic field at the center body of the actuator was measured by a Tesla meter (0−4 A corresponds to 0−130 mT). The digital images and video of the flapping quickly of the butterfly-like actuator under the magnetic field were recorded by a camera. Here, the deflection was defined as the vertical displacement of the end of the wing.

Figure 9 briefly showed the flapping process of the wings of the butterfly-like biomimetic magnetic actuator under the magnetic field. Under increasing magnetic field from 0 to 130 mT, the end of the actuator wings moved from the highest position to the lowest position, which bent into the "flying"

https://doi.org/10.1021/acsami.1c08252
ACS Appl. Mater. Interfaces 2021, 13, 30127−30136

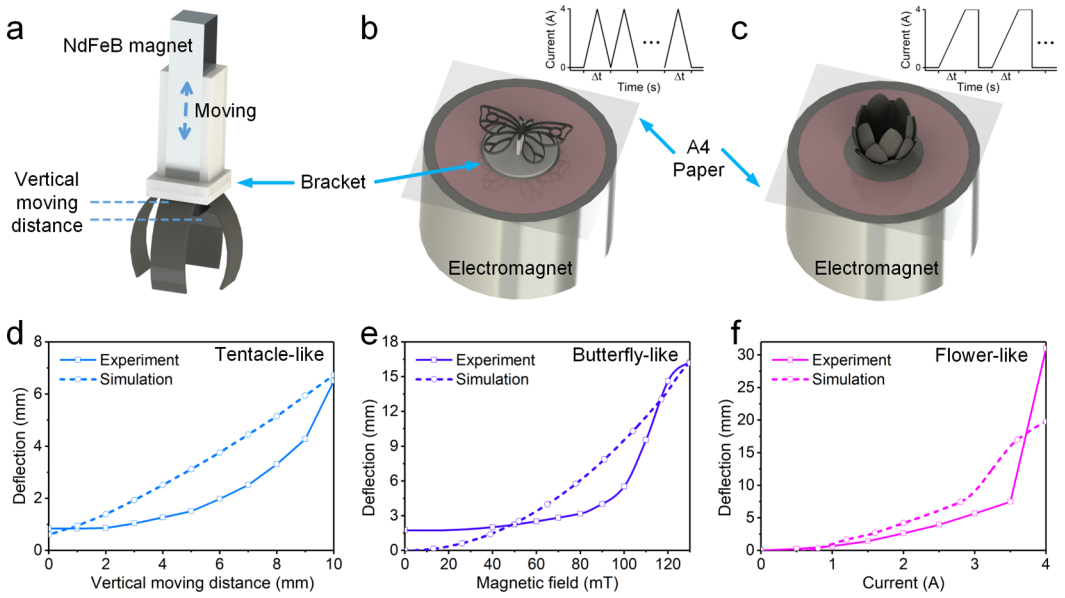

Figure 7. Schematic diagram of the actuation experiment for the (a) tentacle-like biomimetic magnetic actuator, (b) butterfly-like biomimetic magnetic actuator, and (c) flower-like biomimetic magnetic actuator. Experiment and simulation value of the deflection for the (d) tentacle-like actuator, (e) butterfly-like actuator, and (f) flower-like actuator.

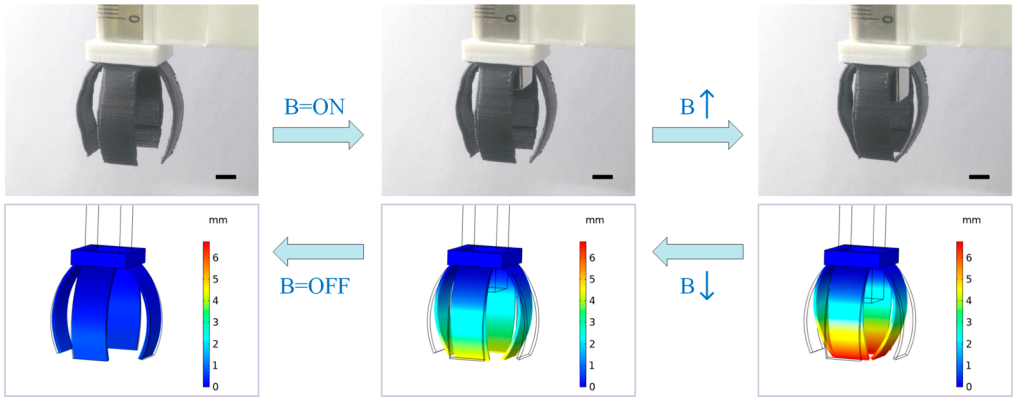

Figure 8. Magnetic field-induced deformation and finite element simulation of the tentacle-like biomimetic magnetic actuator. (scale bar: 5 mm).

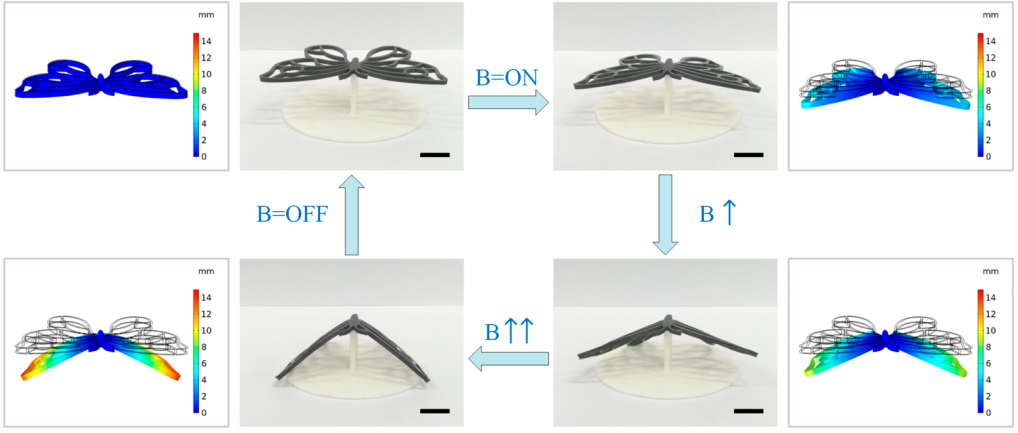

Figure 9. Magnetic field-induced deformation and finite element simulation of the butterfly-like biomimetic magnetic actuator (scale bar: 10 mm).

posture of a real butterfly. After gradually removing the magnetic field, the biomimetic magnetic actuator recovered to the original shape under the action of inherent elasticity. The results showed that the structural evolution of the biomimetic actuator could immediately follow the varying applied magnetic field. The flapping speed was depended on the varying speed of the magnetic field. The repeated flapping used for flying or hovering was successfully imitated by reversible magnetic actuated deformation under the cyclic magnetic fields (Video S2). Furthermore, the deformation process of the biomimetic

https://doi.org/10.1021/acsami.1c08252
ACS Appl. Mater. Interfaces 2021, 13, 30127−30136

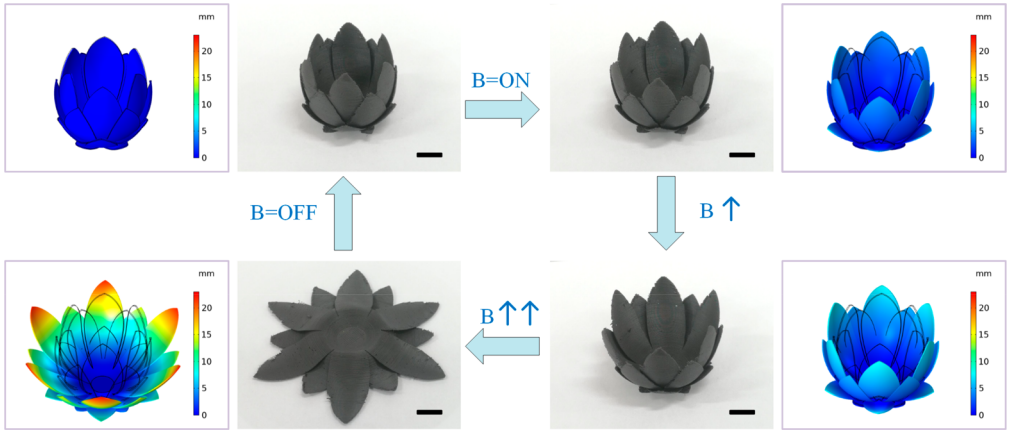

Figure 10. Magnetic field-induced deformation and finite element simulation of the flower-like biomimetic magnetic actuator (scale bar: 10 mm).

actuator could also be analyzed through FEM. The trend between simulated and measured deformation was consistent (Figure 7e), indicating that the finite element analysis model could provide design guidance for the deformation process of 3D printed biomimetic actuators with complex structures. In summary, based on the advantages of rapid prototyping and structural designability, the 3D printed biomimetic magnetic actuators have broad application prospects in the field of soft robotics.

Moreover, a flower-like biomimetic magnetic actuator with different lengths of petals was designed and printed to demonstrate the continuous shape transformation process of the flower. As shown in Figure 7c, the biomimetic actuator was placed directly above the iron core of the electromagnet and deformed under applying the magnetic field. To evaluate the magnetic response behavior of the biomimetic magnetic actuator, the magnetic field-induced deformation process was recorded by a camera. Here, the deflection was defined as the horizontal displacement of the highest point of the petal.

Figure 10 briefly showed the continuous flower blooming behavior of the biomimetic actuator. Upon the small magnetic field, all petals first began to deflect outward to balance the magnetic interaction force. At this stage, due to the large modulus of the materials, the petal deformed slowly and remained straight. With increasing of the magnetic field, the inner petals became unstable, but at this time they were blocked by the outer petals. When the magnetic field was further increased, the outer petals also became unstable, and the entire flower would eventually be locked on the surface of the electromagnet in their deformed shape. After removing the magnetic field, all petals were quickly returned to the original shape, which must be attributed to the inherent elasticity of the materials. The above results showed that the deflection behavior of petals depended on the actuator structure and the applied magnetic field strength. Consistent with the cantilever beam experiment, the petal length had a critical influence on the deformation characteristics. The longer petal was more sensitive to magnetic fields. Besides, the bending and recovery of the actuator could be controlled by the time-varying magnetic field. Under the coupling of magnetic interaction force and elastic force, the flower-like biomimetic magnetic actuator could open the petals directionally (Video S3). Figure 7f also showed the comparison between experimental data and simulated results. Obviously, the variation trend of the simulation and experimental data was consistent, indicating that the established model could describe the magnetic response behaviors. Here, due to the limitation of computational convergence, the model could not fit the large rotational deformation after buckling well. As a result, the model based on the nonlinear solution was effective for explaining the bending deformation of petals and predicting the deflection at low rotation angles, which was useful for the structural design of smart biomimetic actuators.

Obviously, the 3D-printed biomimetic structures can simultaneously combine the advantages of 3D printing (rapid prototyping and convenient structure designability) and the advantages of magneto-active materials (high flexibility, remote noncontact control, and rapid magnetic response properties), which have broad application prospects in the field of the soft robot, biomedicine, and bionics.

4. CONCLUSION

In summary, a 3D printing strategy is developed to fabricate magneto-active actuators by using a flexible magnetic filament. The cantilever beam experiment proved that the printing orientations and layer thickness played a critical role in determining the mechanical properties of the printed structure. The longer and thinner films with the 0° printing orientation were easy to bend and deform, and the maximum deflection of the film (20 × 10 × 0.34 mm) reached 19 mm under a 70 mT magnetic field. Inspired by the movement behavior of natural creatures (octopus tentacles, butterflies, and flowers), several biomimetic magnetic actuators were printed to imitate their motion characteristics. The actuation experiments showed that the printed magnetic actuator possessed programmable integrated structure, rapid prototyping, remote magnetic actuation, fast response capability, and good controllability. Furthermore, the deformation characteristics of the actuators were analyzed by FEM. The results indicated that the variation trend of the simulation value and the experimental value were highly consistent. The effective simulation model could be further used to guide the structural design of the actuator. This research proved the successful application of FDM 3D printing technology in the manufacture of biomimetic actuators based on magneto-active materials, which provided a promising strategy for the structural designability and integrated rapid prototyping of actuators. Obviously, this work has broad application prospects in soft robotics, intelligent devices, bionics, and others fields.

https://doi.org/10.1021/acsami.1c08252
ACS Appl. Mater. Interfaces 2021, 13, 30127−30136

■ ASSOCIATED CONTENT

Supporting Information

The Supporting Information is available free of charge at https://pubs.acs.org/doi/10.1021/acsami.1c08252.

Magnetic actuation deformation of the tentacle-like biomimetic magnetic actuator (MP4)

Magnetic actuation deformation of the butterfly-like biomimetic magnetic actuator (MP4)

Magnetic actuation deformation of the flower-like biomimetic magnetic actuator (MP4)

■ AUTHOR INFORMATION

Corresponding Authors

Shouhu Xuan − *CAS Key Laboratory of Mechanical Behavior and Design of Materials, Department of Modern Mechanics, CAS Center for Excellence in Complex System Mechanics, University of Science and Technology of China, Hefei 230027, China*; orcid.org/0000-0002-8232-9736; Email: xuansh@ustc.edu.cn

Xinglong Gong − *CAS Key Laboratory of Mechanical Behavior and Design of Materials, Department of Modern Mechanics, CAS Center for Excellence in Complex System Mechanics, University of Science and Technology of China, Hefei 230027, China*; orcid.org/0000-0001-6997-9526; Phone: 86-551-63606382; Email: gongxl@ustc.edu.cn; Fax: 86-551-63600419

Authors

Xufeng Cao − *CAS Key Laboratory of Mechanical Behavior and Design of Materials, Department of Modern Mechanics, CAS Center for Excellence in Complex System Mechanics, University of Science and Technology of China, Hefei 230027, China*

Shuaishuai Sun − *Department of Precision Machinery and Instrumentation, University of Science and Technology of China, Hefei 230027, P. R. China*

Zhenbang Xu − *CAS Key Laboratory of On-orbit Manufacturing and Integration for Space Optics System, Changchun Institute of Optics, Fine Mechanics and Physics, Chinese Academy of Sciences, Changchun 130033, P. R. China*

Jun Li − *Anhui Weiwei Rubber Parts Group Co. Ltd., Tongcheng 231400, Anhui, China*

Complete contact information is available at: https://pubs.acs.org/10.1021/acsami.1c08252

Notes

The authors declare no competing financial interest.

■ ACKNOWLEDGMENTS

Financial support from the National Natural Science Foundation of China (Grant Nos. 11822209, 12072338, and 11972343), the Fundamental Research Funds for the Central Universities (WK2480000007 and WK2480000009), Joint Fund of USTC-National Synchrotron Radiation Laboratory (KY2090000055), the Anhui's Key R&D Program of China (202104a05020009), and the Strategic Priority Research Program of the Chinese Academy of Sciences (Grant No. XDB22040502) are gratefully acknowledged.

■ ABBREVIATIONS

FDM, fused deposition modeling; FEM, finite element method; TPR, thermoplastic rubber; CIPs, carbonyl iron particles; DLP, digital light processing; DIW, direct ink writing; SEM, scanning electron microscopy; DMA, dynamic mechanical analyzer

■ REFERENCES

(1) Li, L.; Scheiger, J. M.; Levkin, P. A. Design and Applications of Photoresponsive Hydrogels. *Adv. Mater.* **2019**, *31*, 1807333.

(2) Chen, Y. H.; Yang, J. J.; Zhang, X.; Feng, Y. Y.; Zeng, H.; Wang, L.; Feng, W. Light-Driven Bimorph Soft Actuators: Design, Fabrication, and Properties. *Mater. Horiz.* **2021**, *8*, 728−757.

(3) Shin, Y.; Choi, M.-Y.; Choi, J.; Na, J.-H.; Kim, S. Y. Design of an Electro-Stimulated Hydrogel Actuator System with Fast Flexible Folding Deformation under a Low Electric Field. *ACS Appl. Mater. Interfaces* **2021**, *13*, 15633−15646.

(4) Wang, C. J.; Sim, K.; Chen, J.; Kim, H.; Rao, Z. Y.; Li, Y. H.; Chen, W. Q.; Song, J. Z.; Verduzco, R.; Yu, C. J. Soft Ultrathin Electronics Innervated Adaptive Fully Soft Robots. *Adv. Mater.* **2018**, *30*, 1706695.

(5) Li, Z.; Huang, R.; Liu, Z. A Periodic Deformation Mechanism of a Soft Actuator for Crawling and Grasping. *Adv. Mater. Technol.* **2019**, *4*, 1900653.

(6) Cai, Z.; Song, Z.; Guo, L. Thermo- and Photoresponsive Actuators with Freestanding Carbon Nitride Films. *ACS Appl. Mater. Interfaces* **2019**, *11*, 12770−12776.

(7) Hu, W. Q.; Lum, G. Z.; Mastrangeli, M.; Sitti, M. Small-Scale Soft-Bodied Robot with Multimodal Locomotion. *Nature* **2018**, *554*, 81−85.

(8) Huang, H. W.; Uslu, F. E.; Katsamba, P.; Lauga, E.; Sakar, M. S.; Nelson, B. J. Adaptive Locomotion of Artificial Microswimmers. *Sci. Adv.* **2019**, *5*, No. eaau1532.

(9) Song, H.; Lee, H.; Lee, J.; Choe, J. K.; Lee, S.; Yi, J. Y.; Park, S.; Yoo, J.-W.; Kwon, M. S.; Kim, J. Reprogrammable Ferromagnetic Domains for Reconfigurable Soft Magnetic Actuators. *Nano Lett.* **2020**, *20*, 5185−5192.

(10) Robertson, M. A.; Sadeghi, H.; Florez, J. M.; Paik, J. Soft Pneumatic Actuator Fascicles for High Force and Reliability. *Soft Robot.* **2017**, *4*, 23−32.

(11) Zhang, Y.-F.; Ng, C. J.-X.; Chen, Z.; Zhang, W.; Panjwani, S.; Kowsari, K.; Yang, H. Y.; Ge, Q. Miniature Pneumatic Actuators for Soft Robots by High-Resolution Multimaterial 3D Printing. *Adv. Mater. Technol.* **2019**, *4*, 1900427.

(12) Yan, Y. S.; Santaniello, T.; Bettini, L. G.; Minnai, C.; Bellacicca, A.; Porotti, R.; Denti, I.; Faraone, G.; Merlini, M.; Lenardi, C.; Milani, P. Electroactive Ionic Soft Actuators with Monolithically Integrated Gold Nanocomposite Electrodes. *Adv. Mater.* **2017**, *29*, 1606109.

(13) Tan, H.; Liang, S.; Yu, X.; Song, X.; Huang, W.; Zhang, L. Controllable Kinematics of Soft Polymer Actuators Induced by Interfacial Patterning. *J. Mater. Chem. C* **2019**, *7*, 5410−5417.

(14) Yan, X. H.; Zhou, Q.; Vincent, M.; Deng, Y.; Yu, J. F.; Xu, J. B.; Xu, T. T.; Tang, T.; Bian, L. M.; Wang, Y. X. J.; Kostarelos, K.; Zhang, L. Multifunctional Biohybrid Magnetite Microrobots for Imaging-Guided Therapy. *Sci. Robot.* **2017**, *2*, No. eaaq1155.

(15) Peters, C.; Hoop, M.; Pane, S.; Nelson, B. J.; Hierold, C. Degradable Magnetic Composites for Minimally Invasive Interventions: Device Fabrication, Targeted Drug Delivery, and Cytotoxicity Tests. *Adv. Mater.* **2016**, *28*, 533−538.

(16) Li, Y.; Li, J.; Li, W.; Du, H. A State-of-the-Art Review On Magnetorheological Elastomer Devices. *Smart Mater. Struct.* **2014**, *23*, 123001.

(17) Chai, Z.; Liu, M.; Chen, L.; Peng, Z.; Chen, S. Controllable Directional Deformation of Micro-Pillars Actuated by a Magnetic Field. *Soft Matter* **2019**, *15*, 8879−8885.

(18) Jiralerspong, T.; Bae, G.; Lee, J.-H.; Kim, S.-K. Wireless Control of Two- and Three- Dimensional Actuations of Kirigami Patterns Composed of Magnetic-Particles-Polymer Composites. *ACS Nano* **2020**, *14*, 17589−17596.

(19) Schmauch, M. M.; Mishra, S. R.; Evans, B. A.; Velev, O. D.; Tracy, J. B. Chained Iron Microparticles for Directionally Controlled Actuation of Soft Robots. *ACS Appl. Mater. Interfaces* **2017**, *9*, 11895−11901.

(20) Tang, S. Y.; Zhang, X. C.; Sun, S. S.; Yuan, D.; Zhao, Q. B.; Yan, S.; Deng, L.; Yun, G. L.; Zhang, J.; Zhang, S. W.; Li, W. H. Versatile Microfluidic Platforms Enabled by Novel Magnetorheological Elastomer Microactuators. *Adv. Funct. Mater.* **2018**, *28*, 1705484.
(21) Ho, D. H.; Hong, P.; Han, J. T.; Kim, S.-Y.; Kwon, S. J.; Cho, J. H. 3D-Printed Sugar Scaffold for High-Precision and Highly Sensitive Active and Passive Wearable Sensors. *Adv. Sci.* **2020**, *7*, 1902521.
(22) Zhou, N. J.; Liu, C. Y.; Lewis, J. A.; Ham, D. Gigahertz Electromagnetic Structures via Direct Ink Writing for Radio-Frequency Oscillator and Transmitter Applications. *Adv. Mater.* **2017**, *29*, 1605198.
(23) Rosental, T.; Magdassi, S. A New Approach to 3D Printing Dense Ceramics by Ceramic Precursor Binders. *Adv. Eng. Mater.* **2019**, *21*, 1900604.
(24) Kang, H. W.; Lee, S. J.; Ko, I. K.; Kengla, C.; Yoo, J. J.; Atala, A. A 3D Bioprinting System to Produce Human-Scale Tissue Constructs with Structural Integrity. *Nat. Biotechnol.* **2016**, *34* (3), 312−319.
(25) Xu, T. Q.; Zhang, J. C.; Salehizadeh, M.; Onaizah, O.; Diller, E. Millimeter-Scale Flexible Robots with Programmable Three-Dimensional Magnetization and Motions. *Sci. Robot.* **2019**, *4*, No. eaav4494.
(26) Lantean, S.; Barrera, G.; Pirri, C. F.; Tiberto, P.; Sangermano, M.; Roppolo, I.; Rizza, G. 3D Printing of Magnetoresponsive Polymeric Materials with Tunable Mechanical and Magnetic Properties by Digital Light Processing. *Adv. Mater. Technol.* **2019**, *4*, 1900505.
(27) Ji, Z. Y.; Yan, C. Y.; Yu, B.; Wang, X. L.; Zhou, F. Multimaterials 3D Printing for Free Assembly Manufacturing of Magnetic Driving Soft Actuator. *Adv. Mater. Interfaces* **2017**, *4*, 1700629.
(28) Kim, J.; Chung, S. E.; Choi, S.-E.; Lee, H.; Kim, J.; Kwon, S. Programming Magnetic Anisotropy in Polymeric Microactuators. *Nat. Mater.* **2011**, *10*, 747−752.
(29) Shinoda, H.; Azukizawa, S.; Maeda, K.; Tsumori, F. Bio-Mimic Motion of 3D-Printed Gel Structures Dispersed with Magnetic Particles. *J. Electrochem. Soc.* **2019**, *166*, B3235−B3239.
(30) Joyee, E. B.; Pan, Y. A Fully Three-Dimensional Printed Inchworm-Inspired Soft Robot with Magnetic Actuation. *Soft Robot.* **2019**, *6*, 333−345.
(31) Kim, Y.; Yuk, H.; Zhao, R. K.; Chester, S. A.; Zhao, X. H. Printing Ferromagnetic Domains For Untethered Fast-Transforming Soft Materials. *Nature* **2018**, *558*, 274−279.
(32) Zhu, P. F.; Yang, W. Y.; Wang, R.; Gao, S.; Li, B.; Li, Q. 4D Printing of Complex Structures with a Fast Response Time to Magnetic Stimulus. *ACS Appl. Mater. Interfaces* **2018**, *10*, 36435−36442.
(33) Roh, S.; Okello, L. B.; Golbasi, N.; Hankwitz, J. P.; Liu, J. A. C.; Tracy, J. B.; Velev, O. D. 3D-Printed Silicone Soft Architectures with Programmed Magneto-Capillary Reconfiguration. *Adv. Mater. Technol.* **2019**, *4*, 1800528.
(34) Kim, Y.; Parada, G. A.; Liu, S.; Zhao, X. Ferromagnetic Soft Continuum Robots. *Sci. Robot.* **2019**, *4*, No. eaax7329.
(35) Zhang, Y.; Wang, Q.; Yi, S.; Lin, Z.; Wang, C.; Chen, Z.; Jiang, L. 4D Printing of Magnetoactive Soft Materials for On-Demand Magnetic Actuation Transformation. *ACS Appl. Mater. Interfaces* **2021**, *13*, 4174−4184.
(36) Ma, C.; Wu, S.; Ze, Q.; Kuang, X.; Zhang, R.; Qi, H. J.; Zhao, R. Magnetic Multimaterial Printing for Multimodal Shape Transformation with Tunable Properties and Shiftable Mechanical Behaviors. *ACS Appl. Mater. Interfaces* **2021**, *13*, 12639−12648.
(37) Zhang, F. H.; Wang, L. L.; Zheng, Z. C.; Liu, Y. J.; Leng, J. S. Magnetic Programming of 4D Printed Shape Memory Composite Structures. *Composites, Part A* **2019**, *125*, 105571.
(38) Lin, C.; Lv, J. X.; Li, Y. S.; Zhang, F. H.; Li, J. R.; Liu, Y. J.; Liu, L. W.; Leng, J. S. 4D-Printed Biodegradable and Remotely Controllable Shape Memory Occlusion Devices. *Adv. Funct. Mater.* **2019**, *29*, 1906569.
(39) Qi, S.; Fu, J.; Xie, Y. P.; Li, Y. P.; Gan, R. Y.; Yu, M. Versatile Magnetorheological Plastomer with 3D Printability, Switchable Mechanics, Shape Memory, and Self-Healing Capacity. *Compos. Sci. Technol.* **2019**, *183*, 107817.
(40) Qi, S.; Guo, H. Y.; Fu, J.; Xie, Y. P.; Zhu, M.; Yu, M. 3D Printed Shape-Programmable Magneto-Active Soft Matter for Biomimetic Applications. *Compos. Sci. Technol.* **2020**, *188*, 107973.
(41) Zhao, R.; Kim, Y.; Chester, S. A.; Sharma, P.; Zhao, X. Mechanics of Hard-Magnetic Soft Materials. *J. Mech. Phys. Solids* **2019**, *124*, 244−263.
(42) Boyer, T. H. The Force On a Magnetic Dipole. *Am. J. Phys.* **1988**, *56*, 688−692.
(43) Yin, H. M.; Sun, L. Z. Magnetic Properties of Randomly Dispersed Magnetic Particulate Composites: A Theoretical Study. *Phys. Rev. B: Condens. Matter Mater. Phys.* **2005**, *72*, 054409.

https://doi.org/10.1021/acsami.1c08252
ACS Appl. Mater. Interfaces 2021, 13, 30127−30136